IEEE Photonics Journal
An IEEE Photonics Society Publication

Conditional Frequency-Domain Beamsplitters Using Phase Modulators

Volume 3, Number 5, October 2011

José Capmany
Carlos R. Fernández-Pousa

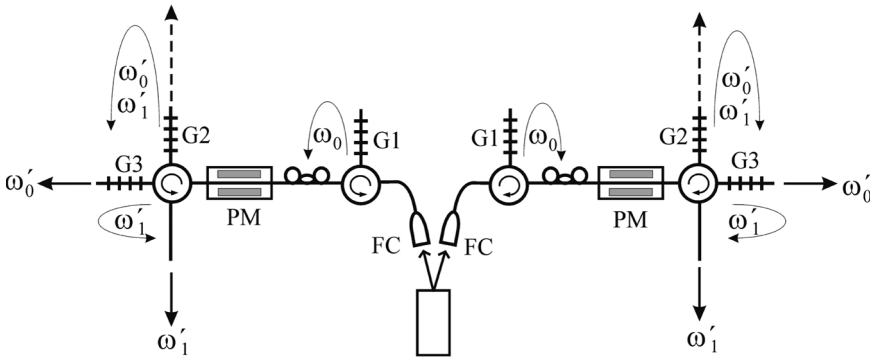

DOI: 10.1109/JPHOT.2011.2170158
1943-0655/$26.00 ©2011 IEEE

IEEE photonics SOCIETY
IEEE

Conditional Frequency-Domain Beamsplitters Using Phase Modulators

José Capmany[1] **and Carlos R. Fernández-Pousa**[2]

[1]ITEAM Research Institute, Universidad Politécnica de Valencia, 46022 Valencia, Spain
[2]Department of Communications Engineering, Universidad Miguel Hernández, 03202 Elche, Spain

DOI: 10.1109/JPHOT.2011.2170158
1943-0655/$26.00 ©2011 IEEE

Manuscript received August 31, 2011; revised September 21, 2011; accepted September 22, 2011. Date of publication September 29, 2011; date of current version October 21, 2011. This paper was supported by the Ministerio de Ciencia y Tecnología, Spain, through Project TEC2008-02606 and through Quantum Optical Information Technology (QOIT): a CONSOLIDER-INGENIO 2010 Project. It is also supported by the Generalitat Valenciana through the PROMETEO 2008/092 research excellency award. Corresponding author: J. Capmany (e-mail: jcapmany@iteam.upv.es).

Abstract: We propose and explore the families of fully tunable, conditional 2×2 frequency-domain beamsplitters that result from sideband coupling in phase modulators. Full tunability is obtained by tailoring the driving voltage feeding the modulators, in a design based on the symmetries of this voltage waveform. The most favorable case in terms of success probability is that of first-sideband coupling, which can be implemented by the use of single-tone phase modulation. The use of this device is illustrated by means of several examples based on the use of a wavelength-routed source of pairs of single-photon frequency-entangled states, showing immediate applications as a means of translating to the frequency-domain quantum-processing protocols based on linear optics.

Index Terms: Quantum information, microwave photonics.

1. Introduction

Quantum optics is recognized as an attractive physical platform for the implementation of quantum information communication and processing systems [1]. The basis of this success lies in the low interactivity of photons with the environment, which is a fact that permits, on the one hand, the remote distribution of quantum states of radiation in free space or guided media and, on the other, to the use of standard photonic devices as controlled interaction regions designed to perform specific quantum processing tasks. Due to the inherent richness in the radiation degrees of freedom, several approaches have been employed to encode and process quantum information by optical means. As the basic information-bearing entity, qubits can be optically encoded with one (single-rail encoding) [2] or two different bosonic modes (dual-rail encoding) of the radiation field [3]. Qubit encoding has been demonstrated with a variety of radiation modes, such as the states of polarization [4], the spatial modes impinging beamsplitters and propagating in interferometers [5], the relative phase between consecutive pulses [6], or different optical frequencies [7].

Frequency modes appear as a natural description of quantum radiation when photon wavepackets with different central frequencies can be resolved in the spectral domain or, alternatively, when broadband radiation is filtered in frequency bins [8], [9]. Their use as an encoding domain brings up two main advantages. On one hand one can profit from the inherent broadband characteristic of optical waveguides. In particular, optical fibers and integrated waveguides provide an immense spectral bandwidth for telecommunications applications, which can also be exploited to accommodate a high number of optical modes for encoding quantum states. This in turn implies that a

high-dimensional Hilbert space is at hand, at least in principle, to support richer computational tasks. A second advantage resides in the fact that many mature photonic technologies and components specifically designed to process individual frequency modes in the context of dense wavelength division multiplexing (DWDM) telecommunications systems can be readily exploited for filtering, multiplexing, demultiplexing, and routing operations required in quantum logic operations supported by this particular encoding alternative.

The manipulation of frequency modes can be realized with optical modulators for providing coupling between frequencies, together with a certain optical filtering technology for selecting and routing different wavelengths. With respect to the modulation techniques, both acousto- [10]–[15] and electrooptic [7], [9], [16] modulators have been used for performing quantum processing tasks. In its simpler configuration, acousto-optic modulators provide a tunable coupling between two different frequencies [12], thus permitting a compact implementation of 2×2 beamsplitters. However, their bandwidth hardly reaches the gigahertz range, thus severely limiting the filtering techniques that can be used in successive processing steps.

By contrast, electrooptic modulators [17] represent an attractive candidate for the implementation of quantum operations involving frequency-domain coding. In first place, they operate as multimode scattering devices where the value of the coupling coefficients between optical frequencies can be controlled and tuned by means of an external control or modulation signal [18], [19]. The key challenge is then to translate this basic functionality onto both simple linear optical operations such as beamsplitting, phase shifting or more complex tasks implemented by means of unitary transformations. In the second place, since current state-of-the art phase modulators feature modulation bandwidths in excess of 50 GHz (even $>$ 100 GHz for polymer devices) for load matched transmission line travelling-wave devices [20]–[22], there is enough room for microwave and even millimeter-wave control signals to be applied. This point is of critical importance in practice since then the modes coupled by the device have enough frequency separation for standard optical filtering technologies to be subsequently interfaced after the device, operating as a mode selection stage. A third advantage is that electrooptic modulation is one of the few functionalities that can be monolithically integrated with waveguides and optical filters in the two main technologies for the implementation of photonic integrated circuits, that is Silicon Photonics [22] and InP [23]. This opens the possibility of developing integrated quantum photonic logic circuits [24], [25] and subsystems which provide further advantages in terms of loss, stability, size, compactness, and cost. Finally, phase modulation technology is available for a wide range of operating wavelengths with commercial devices covering the range between 0.65 and 2 μm [26], [27]. These facts illustrate the importance of considering modulation as a powerful enabling functionality for quantum information systems based on photonic platforms.

In this paper, we explore the optical phase modulator as a candidate for the implementation of quantum operations involving frequency-domain coding, analyzing the operation regimes where the modulator acts as a fully tunable 2×2 frequency beamsplitter (FBS). As a multimode device, the output of phase modulators consists of a number of sideband frequency modes which are created from a single input mode. The use of phase modulators thus requires a postselection of a pair of frequency modes that act as the basic code set, an issue that is analyzed in Section 2. The proper design of FBS, based on single-tone modulation, in treated in Section 3, and in Section 4, we provide a simple optimization strategy for increasing its success probability. In Section 5, we analyze a simple example where phase modulators, used as an FBS, provide pairs of single-photon entangled states in frequency, in an arrangement that mimics standard schemes using pairs of two-photon polarization entangled states or of single-photon entangled states. We also discuss there its use in teleportation and in purification tasks. Finally, we end in Section 6 with our conclusions.

2. Conditional Unitaries From Phase Modulation

In this section, we use standard operator algebra to describe the conditional operation of linear and photon-number preserving systems from two complementary points of view, with particular emphasis

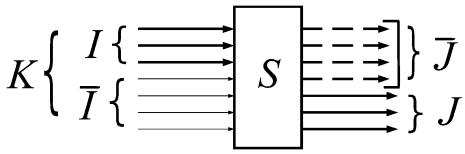

Fig. 1. Scheme of a linear system. The input state is contained in the I modes (thick lines), whereas the modes of the complementary set $\bar{I}$ are in the vacuum state (thin lines). After the interaction, the state is reduced to J modes, and output modes $\bar{J}$ are discarded (thick broken lines followed by a box).

in those operation modes leading to unitary transformations. Here, the postselection is performed in terms of a prescribed set of outgoing modes. The first approach is based on conditional or postselected states and the associated success probabilities, and is naturally formulated in the Schrödinger representation. The second description, which is worked in Heisenberg image, follows from the decomposition of a conditional unitary system as a unitary transformation followed by loss, where the loss accounts for the success probability of the conditional implementation of the unitary. Finally, we specialize these results for the specific case of the frequency modes generated by phase modulators and set the problem of searching for conditional unitaries in terms of the classical Fourier coefficients of the voltage function driving the modulator.

Let us consider a linear system described by its scattering matrix $\hat{S}$, which connects two sets of bosonic input and output modes as depicted in Fig. 1. Modes will be denoted with a lowercase subindex so that $|1_k\rangle = \hat{a}_k^+|0\rangle$ is a one-photon state in mode k, and $|0\rangle$ is the vacuum state. These mode indices are attached to logical input or output ports so that in general, a physical port in the linear system could support both an input and an output logical mode. Uppercase subindices, as those in Fig. 1, denote groups of modes. The total set of input and output modes, eventually infinite in number, is denoted by K. The linear system is assumed to preserve the photon number, and therefore, it can be described by its action over creation operators as

$$\hat{S}\hat{a}_{k'}^+\hat{S}^+ = \sum_{k\in K}\hat{a}_k^+ S_{kk'} \tag{1}$$

where $S_{kk'}$ are the matrix elements of $\hat{S}$ in the one-photon subspace $S_{kk'} = \langle 1_k|\hat{S}|1_{k'}\rangle$.

We will assume that the input states are contained in a certain finite-dimensional set of modes $I \subset K$; the complementary set to I, which we call $\bar{I}$, describes an ancilla in its vacuum state. In general, an input state belonging to a finite-dimensional set of modes I may produce an output state with infinite number of non-vacuum modes. This is the case of phase modulation [27], where modes are indexed by frequency and where states contained in a single frequency mode are transformed into states with infinite number of frequencies. We are interested, however, in schemes where the output is effectively reduced to a finite-dimensional set of modes J, as shown in Fig. 1, where we denote again with a bar its complementary output mode set $J \cup \bar{J} = K$.

The conditional operation of the linear device in Fig. 1 under single-photon inputs can be described as follows. Let us assume that the input is $|\Psi\rangle = \Sigma_{i\in I}\alpha_i|1_i\rangle$ with $\Sigma_{i\in I}|\alpha_i|^2 = 1$. The output photon is thus distributed in the K output modes. Then, the output is

$$\begin{aligned}\hat{S}|\Psi\rangle &= \sum_{i\in I,k\in K}|1_k\rangle S_{ki}\alpha_i \\ &= \sum_{i\in I,j\in J}|1_j\rangle S_{ji}\alpha_i + \sum_{i\in I,j'\in\bar{J}}|1_{j'}\rangle S_{j'i}\alpha_i.\end{aligned} \tag{2}$$

In the last part of the formula, we have separated the outputs in J and $\bar{J}$ modes. The first state in this decomposition, which is denoted $|\Psi'\rangle_J$, is the desired conditional output and is entirely determined by

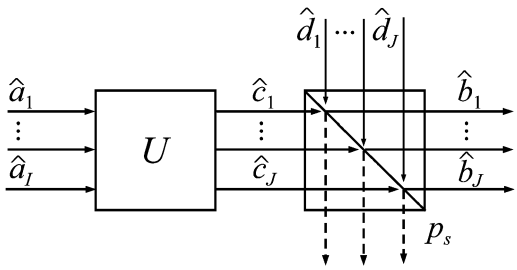

Fig. 2. Equivalent representation of the conditional unitary in terms of a beamsplitter with transmission equal to the success probability p_s.

submatrix $L_{ji} \equiv S_{ji}$, with $j \in J$ and $i \in I$. With this notation, the probability of the generation of a one-photon state $|\Psi'\rangle_J$ is

$$\begin{aligned} \text{Prob}_1 &= {}_J\langle\Psi'|\Psi'\rangle_J \\ &= \left\| \sum_{i\in I, j\in J} |1_j\rangle L_{ji}\alpha_i \right\|^2 \\ &= \sum_{i,k\in I, j\in J} \alpha_k^* L_{jk}^* L_{ji}\alpha_i = (\alpha|L^+L|\alpha) \end{aligned} \tag{3}$$

where the star denotes complex conjugation, and $(\cdot|\cdot)$ denotes the standard scalar product $(\alpha|\beta) = \Sigma_{i\in I}\alpha_i^*\beta_i$. This success probability depends on both the input state and the submatrix L. However, if the dimensionality of I and J coincide and we engineer L to be proportional to an unitary matrix, $L = \sqrt{p_s}U$ with $\sqrt{p_s}$ a positive scalar, the conditional output can be written as

$$|\Psi\rangle_J = \sqrt{p_s} \sum_{i\in I, j\in J} \hat{a}_j^+|0\rangle U_{ji}\alpha_i \equiv \sqrt{p_s}\sum_{i\in I} \alpha_i \hat{c}_i^+|0\rangle \tag{4}$$

with $\hat{c}_m^+$ standard bosonic operators $[\hat{c}_m, \hat{c}_n^+] = \delta_{mn}$. The success probability is then independent of the input $\text{Prob}_1 = p_s$. Therefore, the realization of conditional unitary operations reduces to the identification of submatrices L proportional to unitaries.

Alternatively, the operation of the linear device can be described in Heisenberg image, where the output j modes are given by

$$\begin{aligned} \hat{b}_j \equiv \hat{S}^+\hat{a}_{lj}\hat{S} &= \sum_{k\in K=I\cup\bar{I}} S_{jk}\hat{a}_k \\ &= \sum_{m\in I} L_{jm}\hat{a}_m + \sum_{n\in\bar{I}} S_{jn}\hat{a}_n \equiv \sum_{m\in I} L_{jm}\hat{a}_m + \hat{s}_j \end{aligned} \tag{5}$$

with $\hat{s}_j$ accounting for the coupling with the input $\bar{I}$ vacuum modes. Using the standard bosonic commutation relations for $\hat{a}_m$ and $\hat{b}_j$, we get [26]

$$\left[\hat{s}_p, \hat{s}_q^+\right] = \delta_{pq} - \sum_{n\in J} L_{pn}L_{qn}^*. \tag{6}$$

In the case of L being proportional to an unitary matrix, the vacuum modes can be written as $\hat{s}_j = \sqrt{1-p_s}\,\hat{d}_j$ with $[\hat{d}_m, \hat{d}_n^+] = \delta_{mn}$ so that

$$\hat{b}_j = \sqrt{p_s}\sum_{m\in J} U_{jm}\hat{a}_m + \sqrt{1-p_s}\hat{d}_j = \sqrt{p_s}\hat{c}_j + \sqrt{1-p_s}\hat{d}_j \tag{7}$$

which shows that the linear system acts as the combination of a unitary transformation U followed by a beamsplitter with transmission p_s, as shown in Fig. 2. The probability of successful

transformation of a input state with N photons by unitary U is given by $\text{Prob}_N = p_s^N$; otherwise, some of the photons are lost in the complementary set $\bar{J}$.

The postselection to J can be performed in principle by placing a detector that collects the output modes $\bar{J}$, which is a procedure that implements the detection of the loss port in the equivalent model of Fig. 2. Ideally, the absence of detection validates the postselection, whereas a click detects the exit of at least one photon through the $\bar{J}$ modes. With non-unity detection efficiency and single-photon inputs, failure of detection simply decreases the yield of the postselection, as the output in J would be the vacuum state. However, for inputs with N photons the absence of detection of M photons exiting in $\bar{J}$ would validate a situation where the $N - M$ remaining photons circulate toward J. In this case, the validation of the postselection is to be performed *a posteriori*, by use of a coincidence analysis between N output ports J.

We are interested in the conditional realization of beamsplitters for the specific case of phase modulation, where the device couples modes labeled by frequency. To this end, we focus on a 2-D input mode set I attached to optical frequencies ω_0 and ω_1. For practical reasons, the difference between these frequencies $\omega_1 - \omega_0 > 0$ is assumed to belong to the microwave range (10–40 GHz), since this is the spectral region of operation for which the intersection between efficient mode coupling by phase modulators and mode filtering by photonic components (i.e., Fiber Bragg Gratings and Arrayed Waveguide Gratings) is met by the current state-of-the-art technologies. The mode frequency is denoted as a subindex $|1_\omega\rangle = \hat{a}_\omega^+|0\rangle$. The standard operation regime of phase modulators is with a periodic driving function with angular frequency Ω, so that the device creates, from a certain frequency ω, new frequency modes at $\omega_n = \omega + n\Omega$ with $n = 0, \pm 1, \pm 2, \ldots$ Index n represents the sideband index, and the modulator only couples frequencies separated by $n\Omega$. Therefore, the operation of the modulator is to be designed to provide sideband coupling, i.e., $\omega_1 - \omega_0 = n\Omega$ for some n.

The magnitude of these couplings can be described from the classical driving phase function $x(t)$ [27]. In terms of complex envelopes, the classical transformation induced by phase modulation is

$$A(t) \rightarrow \tilde{A}(t) = A(t)\exp[-ix(t)]. \tag{8}$$

The driving function is periodic $x(t) = x(t + T)$ to provide couplings between modes separated $\Omega = 2\pi/T$, and its Fourier expansion is

$$\exp[-ix(t)] = \sum_{k=-\infty}^{\infty} C_k \exp(-ik\Omega t). \tag{9}$$

Then, the quantum coupling between frequency modes in the optical range is given by the classical Fourier coefficients [27]

$$S_{\omega'\omega} = \langle 1_{\omega'}|\hat{S}|1_\omega\rangle = C_n \tag{10}$$

where $\omega' = \omega + n\Omega$. Then, the scattering matrix of the device can be tailored by an appropriate design of the classical driving function $x(t)$. This freedom, together with a proper selection of the output frequency modes, permits the conditional realization of arbitrary 2×2 unitaries, as is explained in the following sections.

3. Conditional Frequency-Domain 2×2 Beamsplitters

The conditional implementation of frequency-domain 2×2 beamsplitters can be described by means of the layout shown in Fig. 3. Two input optical modes with frequencies ω_0 and ω_1, respectively, are mixed within an electrooptic phase modulator producing two output optical modes of frequencies given by ω_0' and ω_1', which, in general, can be different from ω_0 and ω_1. At the modulator's output, the selection of the two optical mode frequencies is achieved by means of a multiple bandpass optical filter. In the case of the layout shown in Fig. 3, this is performed by a Superimposed Fiber Bragg Grating (SFBG) [28]. With such an arrangement, the presence of a single

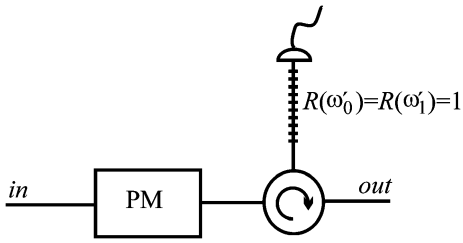

Fig. 3. Circuit layout for the conditional implementation of frequency-domain 2 × 2 beamsplitters. The Fiber Bragg Grating (FBG) is of the superimposed kind (that is, it shows two different bandpass centered at ω_0' y ω_1', respectively, for which the filter reflectance is $R = 1$). A click in the detector placed at the end of the FBG signals the transmission of a photon outside the targeted output modes and, hence, the unsuccessful realization of the beamsplitting operation.

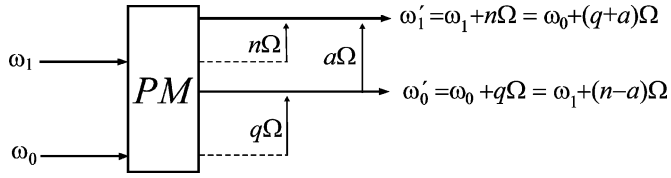

Fig. 4. General diagram showing the coupling between two input frequency modes to two output frequency modes by means of a phase modulator.

photon in any other frequency mode than those corresponding to ω_0, and ω_1 is detected as a click in a photon counter placed at the end of the device.

The general form for the operator L representing the coupling of the two input modes of frequencies ω_0 and ω_1 to the two output modes of frequencies ω_0' and ω_1', as shown in Fig. 4 $(a \neq 0)$, is given by

$$L = \begin{bmatrix} S_{\omega_0'\omega_0} & S_{\omega_1'\omega_0} \\ S_{\omega_0'\omega_1} & S_{\omega_1'\omega_1} \end{bmatrix} = \begin{bmatrix} C_q & C_{q+a} \\ C_{n-a} & C_n \end{bmatrix}. \tag{11}$$

To determine the unitary transformations that can be implemented by means of this transformation, we impose the condition of $L^+ \cdot L$ being proportional to unity. Expressing the transition amplitudes in (11) as $C_q = |C_q|\exp(i\alpha_q)$ this condition transforms to the following identities:

$$\begin{aligned} &|C_q| = |C_n| \\ &|C_{q+a}| = |C_{n-a}| \\ &\alpha_q + \alpha_n = \alpha_{q+a} + \alpha_{n-a} + \pi \qquad \text{mod } 2\pi. \end{aligned} \tag{12}$$

Note that in general, the transition amplitudes or, equivalently, the coefficients in the Fourier expansion of $x(t)$ in (9), can depend on external parameters governing the tunability of the phase modulator. In principle, (12) can be solved for specific values of such external parameters. Nevertheless, we are not interested in these solutions as they do not render parametric solutions for the beamsplitters which could ultimately lead to tunable devices. We will however search for such parametric solutions as a function of modulation functions $x(t)$ fulfilling (12) by means of symmetries. In addition, and as mentioned before, for practical reasons the periodicity of the modulation function $x(t)$ has to be such that $1/T = \Omega/2\pi > 10$ GHz to allow for the implementation of the optical filtering of the output frequency modes using current state-of-the-art technologies. This condition limits the possible options for $x(t)$ since currently available arbitrary waveform generators are limited to clock frequencies of a few gigahertz.

These observations allows us to focus our efforts in parametric families of modulating waveforms $x(t)$ composed of one or two harmonics with variable modulation indexes. More precisely, we

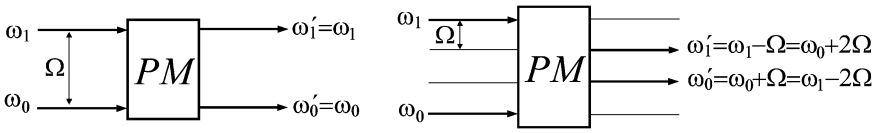

Fig. 5. Diagram showing the frequency band transitions for type A (left, $q = 0$, $a = 1$) and B (right, $q = a = 1$) beamsplitters.

consider here either $x(t)$ functions representing a single tone or generalized $x(t)$ functions verifying the symmetry properties of single-tone modulations, that is, odd symmetry $f(t) = -f(-t)$ and half-wave symmetry $f(t) = -f(t + T/2)$. A more general approach can be followed whereby the two later conditions are verified except for a time shift; therefore, modulation functions $x(t)$ of the form $x(t) = f(t - t_0)$ can be considered. Then the Fourier coefficients of $x(t)$, C_n, are related to those of $f(t)$, which we will denote by D_n, by the following relationship:

$$C_n = e^{i\theta n} D_n \tag{13}$$

being $\theta = -\Omega t_0$. The symmetry properties that $f(t)$ must verify imply, in turn, the following relationships:

$$D_{-n} = (-1)^n D_n, \qquad D_n = D_n^*. \tag{14}$$

Hence, the Fourier coefficients D_n must be real, and moreover, if n is even, there is no phase difference between D_n and D_{-n}, while if n is odd, then the phase difference is π. Then, (13) and (14) imply that $\alpha_n = n\theta + \arg(D_n)$, with $\arg(D_n) = 0$ or π.

In order to solve (12), we first note that the first two identities require that $|q| = |n|$ and $|q + a| = |n - a|$. The first possible solution $\{q = n, q + a = n - a\}$ implies that $a = 0$ and, therefore, must be discarded, while $\{q = n, q + a = a - n\}$ and $\{q = -n, q + a = n - a\}$ imply that either q or $q + a$ must be zero. These conditions are nevertheless a special case of the last possible solution $\{q = -n, q + a = a - n\}$, which only requires that $n = -q$. For this later case, the phase condition in (12) requires, in addition, that a must be odd. The resulting operator matrix is then given by

$$\begin{aligned} L &= \begin{bmatrix} C_q & C_{q+a} \\ C_{-q-a} & C_{-q} \end{bmatrix} \\ &= \begin{bmatrix} e^{i\theta q} D_q & e^{i\theta(q+a)} D_{q+a} \\ (-1)^{q+a} e^{-i\theta(q+a)} D_{q+a} & (-1)^q e^{-i\theta q} D_q \end{bmatrix} \end{aligned} \tag{15}$$

where q is arbitrary and a odd. The corresponding success probability is $p_s = D_q^2 + D_{q+a}^2$.

Equation (15) shows that in these matrices, the output modes represent the $\pm q$ sidebands of each of the input frequency modes. At the same time, these output modes are separated by an odd number a of sidebands. It should be pointed out that from a practical point of view, and especially within the microwave region, it is difficult to achieve high coupling coefficients for sidebands with a high value of sideband index q, and hence, the relevant cases to be considered are those for which $q = 0$, $a = 1$ (which we will call type A beamsplitters), and $q = a = 1$ (type B beamsplitters), as shown in Fig. 5. These cases lead to the following matrices:

$$L_A = \begin{bmatrix} D_0 & e^{i\theta} D_1 \\ -e^{-i\theta} D_1 & D_0 \end{bmatrix}, \quad L_B = \begin{bmatrix} e^{i\theta} D_1 & e^{i2\theta} D_2 \\ e^{-i2\theta} D_2 & -e^{-i\theta} D_1 \end{bmatrix}. \tag{16}$$

We observe that in type A beamsplitters the diagonal elements are in phase, while in the antidiagonal elements, the phase is tunable. On the other hand, type B beamsplitters induce an additional π phase shift in the diagonal elements.

As a first example, we will analyze the frequency-domain beamsplitters that can be implemented using a single radio-frequency tone phase modulation $x(t) = \mu \sin(\Omega t + \theta)$, for which the Fourier

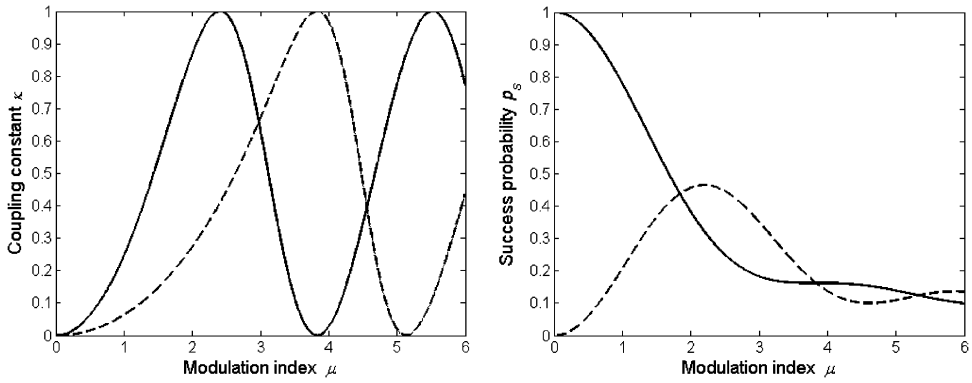

Fig. 6. Coupling constants (left) and success probability (right) for type A (continuous) and type B (broken trace) frequency-domain beamsplitters.

coefficients are given by $C_n = e^{i\theta n} J_n(\mu)$, where J_n is the Bessel function of first kind and order n. In this case, the probabilities of success for the conditional beamsplitting operation are given, respectively, by

$$p_{s,A} = J_0(\mu)^2 + J_1(\mu)^2, \qquad p_{s,B} = J_1(\mu)^2 + J_2(\mu)^2. \tag{17}$$

One can also define, in analogy to the classical optical 2 × 2 coupler [17], the following coupling constants:

$$\kappa_A = \frac{J_1(\mu)^2}{J_0(\mu)^2 + J_1(\mu)^2}, \qquad \kappa_B = \frac{J_2(\mu)^2}{J_1(\mu)^2 + J_2(\mu)^2} \tag{18}$$

which classically determine the amount of power delivered from each input port to its crossed output. The values for p_s and κ as a function of the modulation index μ are represented in Fig. 6. It can be observed, on the one hand, that type A beamsplitters cover the whole range of coupling constant values for values of the modulation index μ between 0 and 2.44, although with a decreasing probability of success (0.27 for $\kappa = 1$). On the other hand, type B beamsplitters feature even lower probabilities of success for the same value of coupling constant, the reason behind this being that type B beamsplitters require the coupling to sidebands of higher order. We conclude that type B beamsplitters and, in general, those involving higher sideband couplings are a less interesting option from the practical point of view. The explicit operator form of the FBS $\hat{U}$ in (7) accounting for the tunable type-A coupling of two frequencies ω_0 and ω_1 is

$$\begin{aligned} \hat{U}(\mu) &= \exp\left[-i\hat{H}_{\omega_o,\omega_1}(\mu)/\hbar\right] \\ \hat{H}_{\omega_o,\omega_1}(\mu) &= i\hbar \sin^{-1}\left[\sqrt{\kappa(\mu)}\right]\left\{e^{j\theta}\hat{a}^{+}_{\omega_o}\hat{a}_{\omega_1} - e^{-j\theta}\hat{a}_{\omega_o}\hat{a}^{+}_{\omega_1}\right\}. \end{aligned} \tag{19}$$

Finally, we point out that the set of 2 × 2 unitary transformations that can be implemented using frequency encoding can be extended by use of a diagonal matrix modifying the phases of the outgoing modes

$$U = \begin{bmatrix} e^{i\beta} & 0 \\ 0 & e^{j\beta'} \end{bmatrix} \begin{bmatrix} \sqrt{1-\kappa} & e^{i\alpha}\sqrt{\kappa} \\ \mp e^{-i\alpha}\sqrt{\kappa} & \pm\sqrt{1-\kappa} \end{bmatrix} \tag{20}$$

which is an extension that can be implemented by use of a dispersive medium where the outgoing photon wavepackets carried at different frequencies undergo different group velocities.

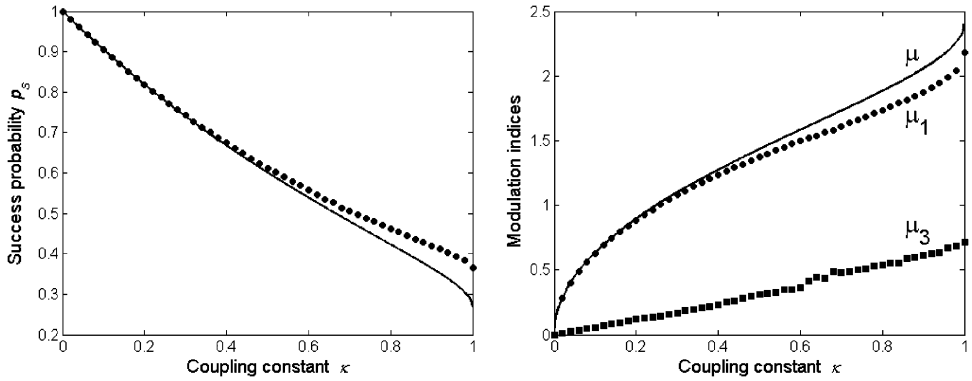

Fig. 7. Probability of success (left) and modulation indices (right) as a function of the coupling constant for single-tone modulation (continuous trace curves) and two optimized modulation tones (dots and squares).

4. Optimization of Conditional Frequency-Domain 2 × 2 Beamsplitters

In a second step within our design process, we will try to improve the probability of success for type A beamsplitters described by (16), which, in the previous section, have been shown to be the most attractive option. This process entails the addition of a second modulation tone at a triple frequency 3 Ω and in phase with the tone at Ω to preserve the aforementioned symmetry properties. Hence, the modulation function is now given by

$$x(t) = \mu_1 \sin(\Omega t + \theta) + \mu_3 \sin(3\Omega t + 3\theta). \tag{21}$$

We first of all proceed to optimize the values of μ_1 y μ_3 to obtain a maximum value for p_s while keeping κ fixed. This can be achieved by adapting a standard optimization procedure used in diffractive optics for the design of Fourier array illuminators [28]. With this aim, we first observe that type A beamsplitters are defined by the moduli of the first Fourier coefficients $|C_0|^2$ and $|C_1|^2 = |C_{-1}|^2$. Ideally, these values must be $(1-\kappa)$ and κ, respectively; nevertheless, in practice, we can only assure that the values of these coefficients will be proportional to the objectives, that is, $|C_0|^2 = \eta(1-\kappa)$ and $|C_1|^2 = \eta\kappa$ for a given constant η. The closest solutions to the ideal one will be those for which the former identities are fulfilled and provide the highest possible value of η. In other words, the objective function to be minimized will be

$$Obj(\mu_1, \mu_3, \eta) = \frac{1}{\eta}\sqrt{\left[|C_1(\mu_1,\mu_3)|^2 - \eta\kappa\right]^2 + \left[|C_0(\mu_1,\mu_3)|^2 - \eta(1-\kappa)\right]^2}. \tag{22}$$

If the objective function achieves a minimum value of zero, then an exact design can be obtained for the beamsplitter of coupling constant κ, and simultaneously, the proportionality constant η will coincide with the probability of success p_s.

Fig. 7 shows in continuous trace the value of p_s versus κ for a single-tone modulation following the first equations in (17) and (18). Dotted curves show similar results for the case of two tone optimized modulation using increments in κ of 0.02. The optimization process has been performed by means of standard minimization routines using a two-step procedure. First, we performed a series of optimizations for each value of κ, using for the seed value of μ_1 as that corresponding to the single-tone modulation case plus 15% random variations, for μ_3 the value 0.5 plus another 15% of random variations, and, for η, a default value $\eta = 0.5$. This permits to easily obtain an estimate of the increase in success probability around the single-tone setting for each value of κ. Then, we refined the best results obtained for each κ. An increment in the probability of success can be observed which is higher for higher values of κ, reaching up to a value of 0.37 for $\kappa = 1$. Despite the fact that this increment may seem moderate, the technique shows a simple and efficient method to improve the versatility of phase modulation.

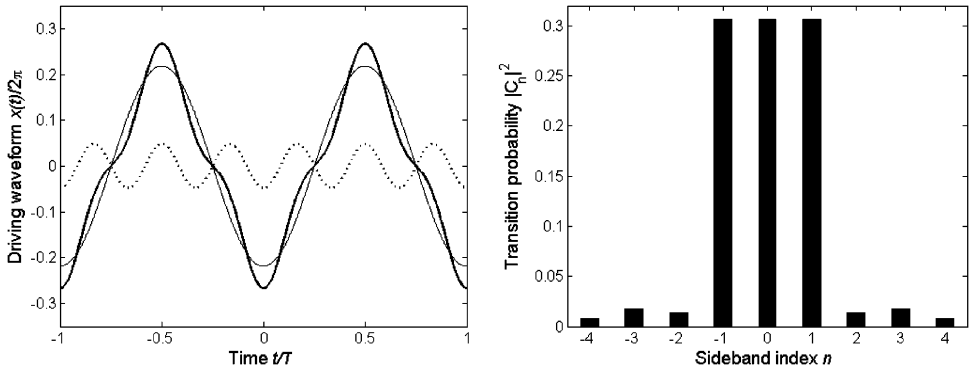

Fig. 8. Modulation waveform $x(t)$ (left) and transition probabilities (right) for a two-tone optimized phase modulation ($\kappa = 0.5$) type A beamsplitter. (Left) In thin black trace is the contribution to the waveform at frequency Ω and in the dotted trace is the contribution at 3 Ω; thick trace is the total waveform.

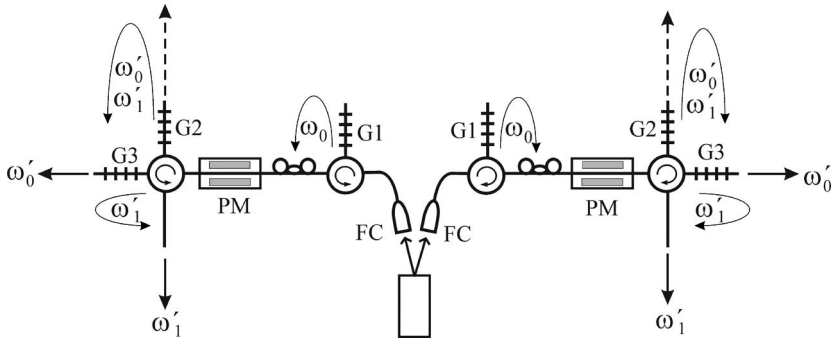

Fig. 9. Scheme of the wavelength-routed source of pairs of frequency-encoded dual-rail qubits.

Finally, as an example, Fig. 8 plots the modulation waveforms and the transition probabilities optimized for the case of $\kappa = 0.5$ for which

$$L_A = \sqrt{\frac{p_s}{2}} \begin{bmatrix} 1 & e^{i\theta} \\ -e^{-i\theta} & 1 \end{bmatrix}. \tag{23}$$

The probability of success for this gate optimized according to (22) is $p_s = 0.61$.

5. A Wavelength-Routed Source of Pairs of Single-Photon Frequency-Entangled States

In this section, we provide some examples of the use of phase modulators as FBS. These examples are based on the schematic platform depicted in Fig. 9, which produces fully tunable pairs of single-photon frequency-entangled states which are additionally routed to four different output ports. This platform can be considered the frequency equivalent to standard setups using coding in spatial modes or in polarization. Referring to that figure, degenerate pairs of single photons are produced by spontaneous parametric down-conversion (SPDC) in a nonlinear crystal and injected into fiber by use of fiber couplers (FC). In order to properly define the initial frequency bin, the SPDC emission is first filtered to a narrow bandwidth $\Delta\omega \ll \Omega$ around the degenerate frequency ω_0, which is a procedure that reduces the spectral distinguishability of signal and idler photons. For Ω in the microwave range (10–40 GHz), frequency bins with bandwidths $\Delta\omega$ in the gigahertz range are thus necessary, for which several filtering techniques can be employed (see [30] and [31]). In Fig. 9, the filtering is schematically implemented by fiber Bragg gratings G1. Alternatively, pairs of indistinguishable single photons can

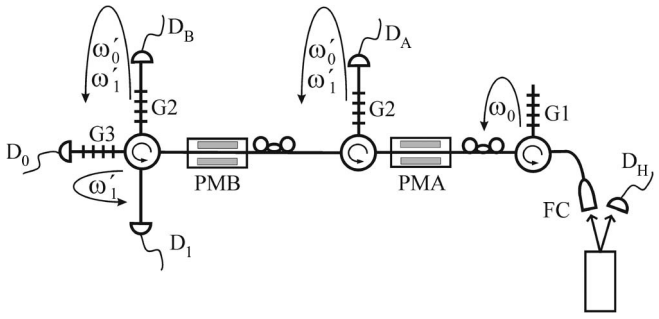

Fig. 10. Scheme for the determination of the fidelity of the generated frequency-encoded qubits using an additional frequency beamsplitter.

be obtained from the consecutive emission of a triggered quantum dot source, which typically have ns wavepacket duration [32]. In either case, we denote the resulting two-photon state as $|1_0\rangle \otimes |1_0\rangle$, where subindices stand for frequency ω_0.

This state is then directed, after polarization alignment, to a pair of phase modulators PM operating independently but with the same driving frequency Ω and output frequencies ω_0' and ω_1'. These output frequencies are first postselected in grating G2 and eventually routed by use of a four-port circulator and gratings G3. The success of the conditional operation of the PM as a FBS can be controlled by detectors at the output of G2 (not shown in the figure), which collect the output PM modes not belonging to the code set $\{\omega_0', \omega_1'\}$. The postselected state is then given by

$$\left[\mu_1 \left|1_0' 0_1'\right\rangle + \nu_1 \left|0_0' 1_1'\right\rangle\right] \otimes \left[\mu_2 \left|1_0' 0_1'\right\rangle + \nu_2 \left|0_0' 1_1'\right\rangle\right] \tag{24}$$

where subindices and primes stand for the outgoing frequencies. State (24) is a pair of single-photon frequency-entangled states or, equivalently, a pair of frequency-encoded dual-rail qubits, where different frequencies have been directed to different physical ports. If standard beamsplitters were used instead of PM [33]–[36], the same state would have been coded in the spatial outgoing ports of the beamsplitters. The proposed system then provides the advantage of using the conditional PM as fully tunable beamsplitters and the fact that the output can be only frequency encoded (when both frequencies are directed to the same output port) or with an additional spatial encoding, routing frequencies to ports, as shown in the figure. We also notice that the polarization-encoded analog of state (24) has been used in quantum processing tasks (see, for instance, [37]), where two polarization-entangled pairs of photons are produced by the double pass of the pump pulse through an SPDC medium.

The determination of the fidelity of the generated single-photon frequency-entangled in the pair state (24) can be performed by adapting to the frequency domain the procedure used in [36]. Referring to Fig. 10, one of the photons in the SPDC pair is directed to detector D_H, which heralds the entrance of a photon in the left conditional generator of a frequency-encoded qubit state implemented by phase modulator PMA. The output frequencies ω_0' and ω_1' are not routed to different ports, and the success of the postselection is determined by the absence of click in detector D_A. For concretion, let us assume that PMA is of type A and creates the maximally frequency-entangled state $|\Psi_+\rangle_{01}' = (1/\sqrt{2})[|1_0' 0_1'\rangle + |0_0' 1_1'\rangle]$. This state is directed to a second PM (PMB) and the postselection success determined by detector D_B. This second FBS acts as a 3-dB coupler $(\kappa = 1/2)$, as described by (23). The exits of PMB at ω_0' and ω_1' are read by detectors D_0 and D_1, respectively. Then, it is straightforward to show that if both the generation in PMA of $|\Psi_+\rangle_{01}'$ and the postselection in PMB succeed, the probability of coincidences between D_H and D_0 (resp. D_H and D_1) is given by $\cos^2(\theta/2)$ (resp. $\sin^2(\theta/2)$), where θ in (23) is the relative phase between zero and first sidebands in type-A FBS. This RF phase θ can be scanned through the PM driving voltage, leading to the corresponding interferogram. If the generation of state $|\Psi_+\rangle_{01}'$ is assumed to suffer from phase damping so that the actual produced state is ρ_{01}', the interferometric visibility V is a measure of the fidelity $F = \langle\Psi_+|\rho|\Psi_+\rangle_{01}' = (1+V)/2$ [36].

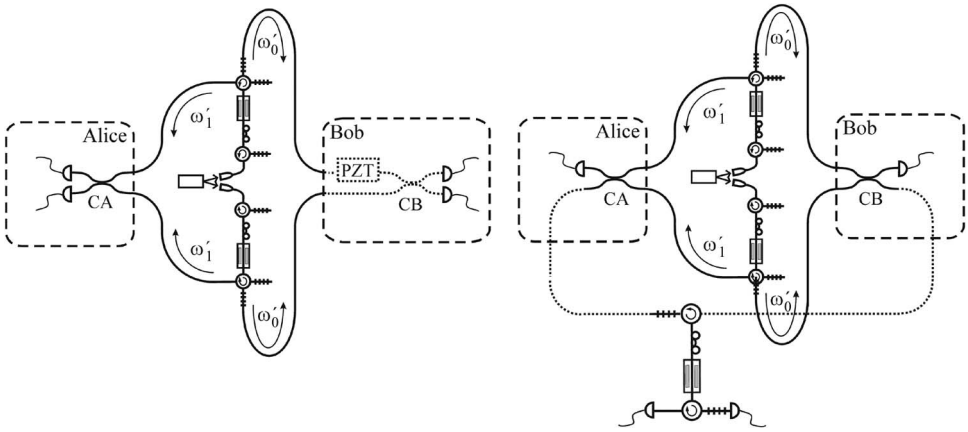

Fig. 11. (Left) Teleportation. (Right) Purification.

The proposed source can be used to translate to frequency encoding other systems based on pairs of entangled single photons encoded in spatial modes. However, the simple substitution of a number of deterministic spatial beamsplitters by conditional FBSs would incur in a progressive decrease of processing rate. This is partly overcome by the wavelength-routing functionality of the system described in Fig. 9, which provides the possibility of distributing state (24) to two locations, i.e., Alice and Bob, where local operations are realized at equal wavelength. In Fig. 11, we briefly present two examples of this architecture. The first of them, which is on the left side of Fig. 11, is an analog of the teleportation experiment of single-photon qubits [33], [34]. A phase modulator is used to create an arbitrary qubit state in dual-frequency basis, whereas the other produces the maximally frequency-entangled state $|\Psi_+\rangle'_{01}$. Then, (24) can be expressed as

$$\begin{aligned}&\left[\mu\left|1'_0 0'_1\right\rangle + \nu\left|0'_0 1'_1\right\rangle\right] \otimes |\Psi_+\rangle'_{01} \\ &\quad = \frac{\mu}{\sqrt{2}}|11\rangle'_0 \otimes |00\rangle'_1 + \frac{\nu}{\sqrt{2}}|00\rangle'_0 \otimes |11\rangle'_1 \\ &\quad + \frac{1}{2}\left[\mu|10\rangle'_0 + \nu|01\rangle'_0\right] \otimes |\Psi_+\rangle'_1 \\ &\quad - \frac{1}{2}\left[\mu|10\rangle_0 - \nu|01\rangle'_0\right] \otimes |\Psi_-\rangle_1 \end{aligned} \tag{25}$$

where $|\Psi_\pm\rangle'_1 = (1/\sqrt{2})[|10\rangle'_1 \pm |01\rangle'_1]$ are maximally entangled single-photon Bell states at frequency ω'_1. Projecting (25) over each of these states at Alice's location by use of the 3-dB coupler CA in Fig. 10 left teleports the qubit state to Bob with $(-)$ or without $(+)$ phase flip. The analysis of the teleportation fidelity can be performed at Bob's site by use of coupler CB and a piezoelectric transducer (PZT) to scan the interferogram.

The second experiment on the right side of Fig. 11 is the frequency-encoded version of the purification protocol of single-photon entangled states reported in [35] and [36]. In this case, the goal is to distribute a single-photon entangled state $|\Psi_+^{ab}\rangle$ between two locations. The channel is assumed to induce phase damping so that we can only distribute

$$\rho_{ab} = F\left|\Psi_+^{ab}\right\rangle\left\langle\Psi_+^{ab}\right| + (1-F)\left|\Psi_-^{ab}\right\rangle\left\langle\Psi_-^{ab}\right| \tag{26}$$

for a certain value of the fidelity F. The protocol of [35] and [36] distributes two copies of state (26) and produces a single copy of the entangled state with increased fidelity. To this end, both copies of (26) are mixed at each location by use of a beamsplitter, whose coupling constant is to be optimized for the initial value of the fidelity and then detect each one of the two output ports of the beamsplitter. As in the teleportation protocol, when only one of the detectors clicks, the reaming modes share a single-photon entangled state with higher fidelity. A simplified version of the protocol fixes the value of the coupling at a values 85/15 and 15/85, attaining a nearly optimal fidelity

improvement for initial $F > 1/2$. In the frequency-encoded version on the right side of Fig. 11, the source is set to create a pair of single-photon frequency-encoded entangled states $|\Phi_+\rangle_{01} \otimes |\Phi_+\rangle_{01}$ and then distributed to Alice and Bob. Notice that the phase-damping channel, which in [36] was implemented by use of two PZTs driven by noise, can be included here in the driving electronics of each PM by simply dithering the phase of the local oscillator with random noise. Once distributed, the protocol proceeds as in the single-frequency case. However, the verification procedure in [36], which is shown in dotted curves in the figure, would require the use of an additional FBS.

6. Conclusion

In this paper, we have explored the families of fully tunable, conditional 2×2 FBSs that result from sideband coupling in phase modulators. Full tunability is obtained by tailoring the driving voltage feeding the modulators in a design based on the symmetries of this voltage waveform. The most favorable case in terms of success probability is that of first-sideband coupling, which can be implemented by use of single-tone phase modulation with a minimum success of 0.27 for maximum coupling $\kappa = 1$. The use of a simple technique employing two microwave tones has been shown to optimize this figure up to a minimum success of 0.37. Finally, the use of this device has been exemplified with the analysis of a wavelength-routed source of pairs of single-photon frequency-entangled states, which shows immediate applications as a means of translating to the frequency-domain quantum-processing protocols based on linear optics.

The advantages of the use of modulation techniques, with basic functionalities such as reconfigurability, wavelength-routing, high bandwidth, and possibility of integration with different filtering and waveguiding technologies, are not exhausted by the examples presented here, which have been based on probabilistic 2×2 unitary transformations. On the one hand, the possibility of configuring different frequency couplings by the driving voltage permits the creation of different families of qudit states coded in frequency. On the other, modulators represent an attractive alternative when both speed and a high degree of reconfigurability are required, such as in recent proposals of linear-optics realizations of channels for multimode qudits [38].

References

[1] T. C. Ralph, "Quantum optical systems for the implementation of quantum information processing," *Rep. Prog. Phys.*, vol. 69, no. 4, pp. 853–898, Apr. 2006.

[2] P. Lund and T. C. Ralph, "Non-deterministic gates for photonic single rail quantum logic," *Phys. Rev. A, Gen. Phys.*, vol. 66, no. 3, p. 032307, Sep. 2002.

[3] I. L. Chuang and Y. Yamamoto, "Simple quantum computer," *Phys. Rev. A, Gen. Phys.*, vol. 52, no. 5, pp. 3489–3496, Nov. 1995.

[4] T. B. Pittman, M. J. Fitch, B. C Jacobs, and J. D. Franson, "Experimental controlled-NOT logic gate for single photons in the coincidence basis," *Phys. Rev. A, Gen. Phys.*, vol. 68, no. 3, p. 032316, Sep. 2003.

[5] J. L. O'Brien, G. J. Pryde, A. G. White, T. C. Ralph, and D. Branning, "Demonstration of an all-optical quantum controlled-NOT gate," *Nature*, vol. 426, no. 6964, pp. 264–267, Nov. 2003.

[6] A. Muller, T. Herzog, B. Huttner, W. Tittel, H. Zbinden, and N. Gisin, "'Plug and play' systems for quantum cryptography," *Appl. Phys. Lett.*, vol. 70, no. 7, pp. 793–795, Feb. 1997.

[7] M. Bloch, S. W. McLaughlin, J.-M. Merolla, and F. Patois, "Frequency-coded quantum key distribution," *Opt. Lett.*, vol. 32, no. 3, pp. 301–303, Feb. 2007.

[8] S. Ramelow, L. Ratschbacher, A. Fedrizzi, N. K. Langford, and A. Zeilinger, "Discrete, tunable color entanglement," *Phys. Rev. Lett.*, vol. 103, no. 25, p. 253601, Dec. 2009.

[9] L. Olislager, J. Cussey, A. T. Nguyen, P. Emplit, S. Massar, J.-M. Merolla, and K. P. Huy, "Frequency bin entangled photons," *Phys. Rev. A, Gen. Phys.*, vol. 82, no. 1, p. 013804, Jul. 2010.

[10] P. C. Sun, Y. Mazurenko, and Y. Fainman, "Long-distance frequency-division interferometer for communication and quantum cryptography," *Opt. Lett.*, vol. 20, no. 9, pp. 1062–1064, May 1995.

[11] A. Stefanov, H. Zbinden, N. Gisin, and A. Suarez, "Quantum entanglement with acousto-optic modulators: Two-photon beatings and Bell experiments with moving beam splitters," *Phys. Rev. A, Gen. Phys.*, vol. 67, no. 4, p. 042115, Apr. 2003.

[12] E. H. Huntington and T. C. Ralph, "Components for optical qubits encoded in sideband modes," *Phys. Rev. A, Gen. Phys.*, vol. 69, no. 4, p. 042318, Apr. 2004.

[13] E. H. Huntington, G. N. Milford, C. Robilliard, T. C. Ralph, O. Glöckl, U. L. Andersen, S. Lorenz, and G. Leuchs, "Demonstration of the spatial separation of the entangled quantum sidebands of an optical field," *Phys. Rev. A, Gen. Phys.*, vol. 71, no. 4, p. 041802, Apr. 2005.

[14] E. H. Huntington, G. N. Milford, C. Robilliard, and T. C. Ralph, "Coherent analysis of quantum optical sideband modes," *Opt. Lett.*, vol. 30, no. 18, pp. 2481–2483, Sep. 2005.
[15] N. S. Jones and T. M. Stace, "Photon frequency-mode matching using acousto-optic frequency beamsplitters," *Phys. Rev. A, Gen. Phys.*, vol. 73, no. 3, p. 033813, Mar. 2006.
[16] J.-M. Merolla, Y. Mazurenko, J.-P. Goedgebuer, L. Duraffourg, H. Porte, and W. T. Rhodes, "Quantum cryptographic device using single-photon phase modulation," *Phys. Rev. A, Gen. Phys.*, vol. 60, no. 3, pp. 1899–1905, Sep. 1999.
[17] A. Yariv and P. Yeh, *Photonics: Optical Electronics in Modern Communications,* 6th ed., Oxford, U.K.: Oxford Univ. Press, 2006.
[18] A. Mahapatra and E. J. Murphy, "Electro-optic modulators," in *Optical Fiber Telecommunications IV*, I. Kaminow and T. Li, Eds. San Diego, CA: Academic, 2002, pp. 258–294.
[19] F. Heismann, S. K. Korotky, and J. J. Veselka, "Lithium niobate integrated optics: Selected contemporary devices and system applications," in *Optical Fiber Telecommunications III*, I. P. Kaminow and T. L. Koch, Eds. San Diego, CA: Academic, 1997, pp. 377–462.
[20] M. Howerton and W. K. Burns, "Broadband travelling wave modulators in $LiNbO_3$," in *RF Photonic Technology in Optical Fiber Links*, W. S. Chang, Ed. Cambridge, U.K.: Cambridge Univ. Press, 2002.
[21] G. E. Betts, "$LiNbO_3$ external modulators and their use in high performance analog links," in *RF Photonic Technology in Optical Fiber Links*, W. S. Chang, Ed. Cambridge, U.K.: Cambridge Univ. Press, 2002.
[22] A. Liu, R. Jones, L. Liao, D. Samara-Rubio, D. Rubin, O. Cohen, R. Nicolaescu, and M. Paniccia, "A high-speed silicon optical modulator based on a metal–oxide–semiconductor capacitor," *Nature*, vol. 427, no. 6975, pp. 615–618, Feb. 2004.
[23] R. Wang, A. Bhardwaj, S. Ristic, L. Coldren, J. Bowers, P. Herczfeld, and Y. Li, "Highly linear InP phase modulator for high dynamic range RF/photonic links," presented at the IEEE Int. Microwave Symp., Anaheim, CA, May 23–28, 2010, Paper WE3C-1.
[24] D. W. Berry and H. M. Wiseman, "Quantum photonics: Quantum optics on a chip," *Nat. Photon.*, vol. 3, no. 6, pp. 317–319, Jun. 2009.
[25] A. Politi, J. Matthews, M. G. Thompson, and J. L. O'Brien, "Integrated quantum photonics," *IEEE J. Sel. Topics Quantum Electron.*, vol. 15, no. 6, pp. 1673–1684, Nov./Dec. 2009.
[26] H. A. Haus, *Electromagnetic Noise and Quantum Optical Measurements*. Berlin, Germany: Springer-Verlag, 2000.
[27] J. Capmany and C. R. Fernández-Pousa, "Quantum modelling of electro-optic modulators," *Laser Photon. Rev.*, vol. 5, Nov. 2011, DOI: 10.1002/lpor.201000038, to be published.
[28] M. Ibsen, M. K. Durkin, M. J. Cole, and R. I. Laming, "Sinc-sampled fiber Bragg gratings for identical multiple wavelength operation," *IEEE Photon. Technol. Lett.*, vol. 10, no. 6, pp. 842–844, Jun. 1998.
[29] J. N. Mait, "Fourier array generators," in *Micro-Optics: Elements, Systems and Applications*, H. P. Herzig, Ed. London, U.K.: Taylor & Francis, 1997.
[30] J.-L. Smirr, S. Guilbaud, J. Ghalbouni, R. Frey, E. Diamanti, R. Alléaume, and I. Zaquine, "Simple performance evaluation of pulse spontaneous parametric down-conversion sources for quantum communications," *Opt. Express*, vol. 19, no. 2, pp. 616–627, Jan. 2011.
[31] M. Halder, A. Beveratos, R. T. Thew, C. Jorel, H. Zbinden, and N. Gisin, "High coherence photon pair source for quantum communication," *New J. Phys.*, vol. 10, no. 2, p. 023027, Feb. 2008.
[32] C. Santori, D. Fattal, J. Vučković, G. S. Solom, and Y. Yamamoto, "Indistinguishable photons from a single-photon device," *Nature*, vol. 419, no. 6907, pp. 594–597, Oct. 2002.
[33] E. Lombardi, F. Sciarrino, S. Popescu, and F. de Martini, "Teleportation of a vacuum-one photon qubit," *Phys. Rev. Lett.*, vol. 88, no. 7, p. 070402, Feb. 2002.
[34] D. Fattal, E. Diamanti, K. Inoue, and Y. Yamamoto, "Quantum teleportation with a quantum dot single photon source," *Phys. Rev. Lett.*, vol. 92, no. 3, p. 037904, Jan. 2004.
[35] N. Sangouard, C. Simon, T. Coudreau, and N. Gisin, "Purification of single-photon entanglement with linear optics," *Phys. Rev. A, Gen. Phys.*, vol. 78, no. 5, p. 050301(R), Nov. 2008.
[36] D. Salar, O. Landry, N. Sangouard, N. Gisin, H. Herrmann, B. Sanguinetti, C. Simon, W. Sohler, R. T. Thew, A. Thomas, and H. Zbinden, "Purification of single-photon entanglement," *Phys. Rev. Lett.*, vol. 104, no. 18, p. 180504, May 2010.
[37] J. W. Pan, M. Danieel, S. Gasparoni, G. Weihs, and A. Zeilinger, "Experimental demonstration of four-photon entanglement and high-fidelity teleportation," *Phys. Rev. Lett.*, vol. 86, no. 20, pp. 4435–4438, May 2001.
[38] M. Piani, D. Pitkanen, R. Kaltenbaek, and N. Lütkenhaus, "Linear-optics realization of channels for single-photon multimode qudits," *Phys. Rev. A, Gen. Phys.*, vol. 84, no. 3, p. 032304, Sep. 2011.